Comparison of Quasi-Static and Exact Electromagnetic Fields from a Horizontal Electric Dipole Above a Lossy Dielectric Backed by an Imperfect Ground Plane

JUAN R. MOSIG AND TAPAN K. SARKAR, SENIOR MEMBER, IEEE

Abstract — **In most microstirp transmission lines, analysis is made assuming that a quasi-TEM mode exists and propagates down the line. The primary objective of this paper is to obtain the region of validity of this assumption. The second objective of this paper is to derive the expressions for the fields for a horizontal electric dipole over a lossy dielectric medium backed by an imperfect ground plane. It is shown that, to a first approximation, fields at the air–dielectric interface are independent of the ground plane conductivity. Since we are interested in coupling between lines, our interest is in the computation of the fields primarily at the air–dielectric interface. Finally, numerical results are presented to show where the quasi-static approximations deviate from the exact solution for a given microstrip geometry as the frequency of operation or the observation point is changed.**

I. Introduction

MICROSTRIP structures are now widely used in computer systems for propagating electrical energy from a source to a load. While almost all microstrip structures have been analyzed by assuming a quasi-TEM model, it is not known *a priori* under what conditions the quasi-TEM model breaks down. Rigorous microstrip formulation for the dynamical case can be established by using well-known stratified media theory. The pioneering study on electromagnetic wave propagation in stratified media must be ascribed to Sommerfeld, who investigated the radio wave propagation above a lossy ground as early as 1909. Later several authors [1]–[3] have extended these theories to arbitrary stratified media, and quite recently this model has been applied to practical microstrip structures [4]–[8].

Even though the Sommerfeld theory yields an exact solution, the analysis is quite complicated, even for the simple case of a horizontal electric dipole over a stratified medium [9]–[10]. That is why a quasi-TEM approximation is often made of the fields that are produced by the dipole.

It is quite apparent that for a given microstrip configuration, if the frequency is low enough, a quasi-TEM analysis would yield a good solution. However, as the frequency of operation increases or as one moves away from the source, the quasi-TEM analysis would tend to differ from the exact analysis. The objective of this paper is to describe the region of validity of the quasi-TEM analysis for a given microstrip configuration. It is important to know the fields at the air–dielectric interface as these fields are primarily responsible for the cross-talk coupling between different microstrip lines. Also, at this interface surface waves are generated. The quasi-TEM analysis neglects the presence of the surface waves. However, if the frequency is high enough or the point of observation is away from the source, it is the surface waves where most of the traveling energy is confined to rather than in the quasi-TEM fields.

This paper reviews the theoretical foundation of a microstrip dynamical model and computes the fields at the interface. Particular attention is paid to the development of efficient numerical techniques. In Section II, the mathematical foundation is reviewed. The expressions for the electric field are presented in Section III. In Section IV, the effect of a finitely conducting ground plane on the field components is taken into account. In Section V, the quasi-static approximations are presented. The computational and numerical details for the evaluation of the fields are described in Section VI. Finally, numerical results are presented in Section VII to outline the regions of validity of the quasi-static approximation.

II. Horizontal Electrical Dipole on Microstrip

Consider a x-directed horizontal electric dipole (HED) of moment Idx located in the air–dielectric interface of a microstrip structure with infinite transverse directions as shown in Fig. 1. The substrate is a homogeneous isotropic

Manuscript received May 20, 1985; revised November 18, 1985. This work was supported by the Digital Equipment Corp. and E. I. Dupont Connector Systems.

J. R. Mosig is with Ecole Polytechnique Federale de Lausanne, CH-1007, Lausanne, Switzerland.

T. K. Sarkar is with the Department of Electrical and Computer Engineering, Syracuse University, Syracuse, NY 13210.

IEEE Log Number 8407179.

0018-9480/86/0400-0379$01.00 ©1986 IEEE

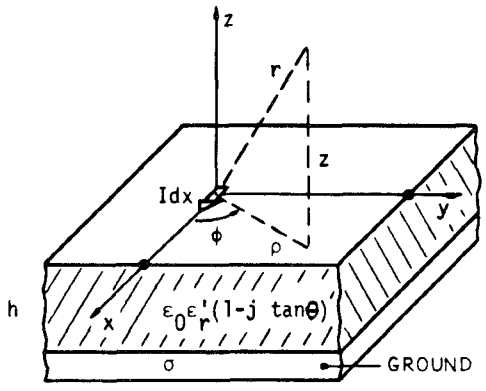

Fig. 1. Geometry of the problem.

lossy dielectric of thickness h and complex permittivity

$$\epsilon = \epsilon_0\epsilon_r = \epsilon_0\epsilon_r'(1 - j\tan\theta) \tag{1}$$

where $\tan\theta$ is the loss tangent and ϵ_r is the complex relative dielectric constant of the medium.

The origin of the coordinate system is chosen to be the location of the HED. The ground plane is located at $z = -h$ and is considered to be a perfectly conducting plane. Later on, this restriction will be removed and the effect of a finite ground plane conductivity will be taken into account.

Following Harrington [10], the electromagnetic fields in such a structure can be derived from a scalar and a vector potential as

$$\boldsymbol{E} = -j\omega\boldsymbol{A} - \nabla V \tag{2}$$

$$\boldsymbol{H} = \frac{1}{\mu_0}\nabla \times \boldsymbol{A}. \tag{3}$$

Several other approaches to determine the fields, such as decomposition into their TM and TE parts, are also currently used [3]–[4]. But the use of potentials is preferred here, because it allows a simple derivation of quasi-static approximations and leads to the well-behaved mixed-potential integral equation.

Both the vector and scalar potentials are solutions of Helmoltz-type equations whose general solution in cylindrical coordinates is, assuming a time dependence of the form $\exp(j\omega t)$

$$\int_C H_n^{(2)}(k_\rho\rho)\left[A_1 e^{jn\phi} + A_2 e^{-jn\phi}\right]\left[B_1 e^{-jk_z z} + B_2 e^{jk_z z}\right] dk_\rho \tag{4}$$

where k_ρ and k_z are the complex radial and vertical component of the wave number

$$k^2 = \omega^2\mu\epsilon = k_\rho^2 + k_z^2 \tag{5}$$

and ρ, ϕ, and z are the descriptions of the cylindrical coordinates. C is an infinite path going from the third to the first quadrant in the complex plane $k_\rho = \lambda + j\nu$ as shown in Fig. 2 [11].

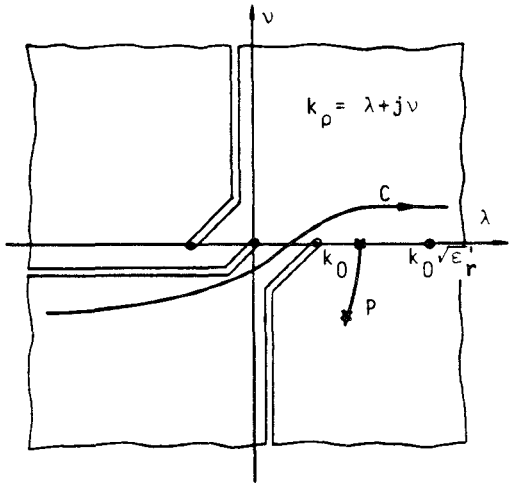

Fig. 2. The complex $\delta_\rho = \lambda + j\nu$ plane with pertinent branch cuts. C = integration path; P = locus of the first pole $\lambda_p + j\nu_p$ as a function of dielectric losses.

The boundary conditions for tangential fields in microstrip structure are

$$\left.\begin{aligned} \boldsymbol{e}_z \times (\boldsymbol{E}_1 - \boldsymbol{E}_2) &= 0 \\ \boldsymbol{e}_z \times (\boldsymbol{H}_1 - \boldsymbol{H}_2) &= \boldsymbol{J}_s \end{aligned}\right\} \quad \text{at interface } z = 0 \tag{6, 7}$$

$$\left.\begin{aligned} \boldsymbol{e}_z \times \boldsymbol{E}_2 &= 0 \\ \boldsymbol{e}_z \times \boldsymbol{H}_2 &= \boldsymbol{J}_s \end{aligned}\right\} \quad \text{at the ground plane } z = -h \tag{8, 9}$$

where indexes 1 and 2 refer to air and dielectric substrate, respectively. Conditions (6)–(8) suffice to obtain the potentials. Equation (9) can be used to determine the currents in the ground plane.

The surface current associated with an HED is given by the Dirac's Delta distribution

$$\boldsymbol{J}_s = \boldsymbol{e}_x \frac{\delta(\rho)}{2\pi\rho} I\,dx$$

$$= \boldsymbol{e}_x \frac{I\,dx}{4\pi}\int_C H_0^{(2)}(k_\rho\rho)\,k_\rho\,dk_\rho, \qquad z = 0 \tag{10}$$

where the Hankel transform for $\delta(\rho)/\rho$ has been utilized in (10).

It is well known [3]–[7] that two components for the magnetic vector potential A_x and A_z are needed to satisfy the boundary conditions (6)–(8). For both the potentials, the boundary conditions transform to

$$\left.\begin{aligned} V_1 &= V_2 \\ \boldsymbol{A}_1 &= \boldsymbol{A}_2 \\ \frac{\partial A_{x_1}}{\partial z} - \frac{\partial A_{x_2}}{\partial z} &= -\mu_0 J_x \end{aligned}\right\}, \quad \text{on } z = 0 \tag{11, 12, 13}$$

and

$$\left.\begin{aligned} V_2 &= 0 \\ A_{x_2} &= 0 \\ \frac{\partial A_{z_2}}{\partial z} &= 0. \end{aligned}\right\}, \quad \text{on } z = -h. \tag{14, 15, 16}$$

Introducing the above conditions (11)–(16) and utilizing the general expression (4), we obtain for the potentials

$$\begin{Bmatrix} A_{x_1} \\ A_{x_2} \end{Bmatrix} = \frac{\mu_0}{4\pi} I\,dx \int_C H_0^{(2)}(k_\rho \rho) \frac{k_\rho}{D_H} \begin{Bmatrix} \exp(-u_0 z) \\ \dfrac{\sinh u(z+h)}{\sinh uh} \end{Bmatrix} dk_\rho \tag{17}$$

$$\begin{Bmatrix} A_{z1} \\ A_{z2} \end{Bmatrix} = -\frac{\mu_0}{4\pi} I\,dx(\epsilon_r - 1)\cos\phi \cdot \int_C H_1^{(2)}(k_\rho \rho) \frac{k_\rho^2 N}{D_H D_E} \begin{Bmatrix} \exp(-u_0 z) \\ \dfrac{\cosh u(z+h)}{\cosh uh} \end{Bmatrix} dk_\rho \tag{18}$$

and

$$\begin{Bmatrix} V_1 \\ V_2 \end{Bmatrix} = \frac{\cos\phi}{4\pi j\omega\epsilon_0} I\,dx \cdot \int_C H_1^{(2)}(k_\rho \rho) \frac{k_\rho^2 N}{D_H D_E} \begin{Bmatrix} \exp(-u_0 z) \\ \dfrac{\sinh u(z+h)}{\sinh uh} \end{Bmatrix} dk_\rho \tag{19}$$

where

$$u_0 = jk_{z0} = \sqrt{k_\rho^2 - k_0^2} \tag{20}$$

$$u = jk_z = \sqrt{k_\rho^2 - \epsilon_r k_0^2} \tag{21}$$

$$k_0^2 = \omega^2 \mu_0 \epsilon_0 \tag{22}$$

and the functions D_H, D_E, and N are given by

$$D_H = u_0 + u\coth uh \tag{23}$$

$$D_E = \epsilon_r u_0 + u\tanh uh \tag{24}$$

$$N = u_0 + u\tanh uh. \tag{25}$$

In particular, D_H and D_E are closely linked to the Fresnel reflection coefficients R_H and R_E of a TE(H) or TM(E) wave [3], respectively, by the relations

$$R_H = \frac{2u_0}{D_H} - 1 \tag{26}$$

$$R_E = \frac{2\epsilon_r u}{D_E} - 1. \tag{27}$$

Thus, the zeros of D_H and D_E give the phase constant of the characteristic TE and TM surface wave modes propagating in such a structure [4]–[7]. For a lossless substrate, the zeros are situated on the segment $\{[k_0], [\sqrt{\epsilon_r} k_0]\}$ of the real axis $\lambda = \mathrm{Re}\,[k_\rho]$, as shown in Fig. 2. For the lossy case, the zeros move away from the real axis, thereby having a small negative imaginary part.

As could be expected, the A_z component vanishes when $\epsilon_r = 1$. The sources of the scalar potential V are the charges associated with the HED via the continuity equation, namely, two point changes of value $q = \pm I/j\omega$ separated by an infinitesimal distance dx. The scalar potential V_q of a unit point change is related to the scalar potential of a HED via the relationship

$$V = \frac{I\,dx}{j\omega} \cdot \frac{\partial V_q}{\partial x}. \tag{28}$$

III. Expressions for the Fields

The electromagnetic field is now derived from the potentials by using (2) and (3). For the sake of completeness, here are the complete expressions for the six cartesian components of the fields at the air–dielectric interface

$$4\pi j\omega\epsilon_0 E_x = I\,dx \left[k_0^2 \int_C H_0^{(2)}(k_\rho \rho) \frac{k_\rho}{D_H} dk_\rho + \frac{\cos 2\phi}{\rho} \int_C H_1^{(2)}(k_\rho \rho) \frac{k_\rho^2 N}{D_H D_E} dk_\rho - \cos^2\phi \int_C H_0^{(2)}(k_\rho \rho) \frac{k_\rho^3 N}{D_H D_E} dk_\rho \right] \tag{29}$$

$$4\pi j\omega\epsilon_0 E_y = I\,dx \sin 2\phi \left[\frac{1}{\rho} \int_C H_1^{(2)}(k_\rho \rho) \frac{k_\rho^2 N}{D_H D_E} dk_\rho - 1/2 \int_C H_0^{(2)}(k_\rho \rho) \frac{k_\rho^3 N}{D_H D_E} dk_\rho \right] \tag{30}$$

$$4\pi j\omega\epsilon_0 E_z = I\,dx \cos\phi \int_C H_1^{(2)}(k_\rho \rho) \cdot \frac{k_\rho^2 u \tanh uh}{D_E} dk_\rho \tag{31}$$

$$4\pi H_x = I\,dx(\epsilon_r - 1)\sin 2\phi \cdot \left[\frac{1}{\rho} \int_C H_1^{(2)}(k_\rho \rho) \frac{k_\rho^2}{D_E D_H} dk_\rho - 1/2 \int_C H_0^{(2)}(k_\rho \rho) \frac{k_\rho^3}{D_E D_H} dk_\rho \right] \tag{32}$$

$$4\pi H_y = -I\,dx \int_C H_0^{(2)}(k_\rho \rho) \frac{k_\rho u_0}{D_H} dk_\rho + I\,dx(\epsilon_r - 1) \left[\cos^2\phi \int_C H_0^{(2)}(k_\rho \rho) \cdot \frac{k_\rho^3}{D_E D_H} dk_\rho - \frac{\cos 2\phi}{\rho} \cdot \int_C H_1^{(2)}(k_\rho \rho) \frac{k_\rho^2}{D_E D_H} dk_\rho \right] \tag{33}$$

$$4\pi H_z = I\,dx \sin\phi \int_C H_1^{(2)}(k_\rho \rho) \frac{k_\rho^2}{D_H} dk_\rho. \tag{34}$$

As expected, the H_x component vanishes for the case $\epsilon_r = 1$. Also, the E_z component is discontinuous at $z = 0$,

since permittivity changes. The above expression corresponds to the value of the field in the air at $z = 0+$.

IV. Effect of a Finite Conductivity Ground Plane

A finite conductivity ground plane can be modelled as an impedance wall where

$$\boldsymbol{E}_{\tan} = Z_s \boldsymbol{J}_s = Z_s(\boldsymbol{e}_z \times \boldsymbol{H}_{\tan}) \tag{35}$$

with Z_s being the surface impedance

$$Z_s = \frac{1+j}{\sigma\delta}, \qquad \delta = \text{skin depth}, \qquad \sigma = \text{conductivity}. \tag{36}$$

The exact solution of the microstrip problem with the condition (35) replacing (8) is quite involved [1], [3]. For small ohmic losses a perturbation technique similar to the one used to calculate attenuation factors in waveguides can be used. Thus the magnetic field in (35) is approximated by its value in the infinite conductivity case (32)–(34).

The new set of boundary conditions for the potentials are identical at the interface, but in the ground plane, we have

$$V_2 = 0 \tag{37}$$

$$A_{x2} = \frac{Z_s}{j\omega} H_{y2}(\sigma = \infty) \tag{38}$$

$$\frac{\partial A_{z2}}{\partial z} = -\frac{Z_s}{j\omega}\frac{\partial H_{y2}}{\partial x}(\sigma = \infty). \tag{39}$$

The potentials are now obtained from (11)–(13) and (37)–(39).

To illustrate the effect of a finite conductivity in a situation of practical interest, let us consider the tangential electric field at the interface.

The relevant potentials are A_x and V, since

$$E_x = -j\omega A_x - \frac{\partial V}{\partial x} \quad \text{and} \quad E_y = -\frac{\partial V}{\partial y}.$$

We obtain

$$A_x = \frac{\mu_0}{4\pi} I\,dx \int_C H_0^{(2)}(k_\rho \rho) \cdot \frac{k_\rho}{D_H}\left[1 - \frac{jRu\exp(-uh)}{k_0 \sinh uh}\right] dk_\rho \tag{40}$$

$$V = \frac{I\,dx\cos\phi}{4\pi j\omega\epsilon_0} \int_C H_1^{(2)}(k_\rho \rho) \cdot \frac{N + jk_0(\epsilon_r - 1)R\exp(-uh)}{D_H D_E \cosh uh} k_\rho^2\, dk_\rho \tag{41}$$

where R is the ratio between the surface impedance and the free space impedance

$$R = \frac{Z_s}{Z_0} = (1+j)\sqrt{\frac{\pi f \epsilon_0}{\sigma}} \tag{42}$$

and f is the frequency of operation. By comparing with the expressions for the potentials in the perfect ground plane case, we observe that the difference is in the one additional term in the numerator for the potentials. This term is proportional to the ratio R between surface impedance and free-space impedance. In addition, for the scalar potential the term is proportional to the difference $(\epsilon_r - 1)$.

However, the poles of the integrands in the potential expressions are still given by the zeros of D_H and D_E. Hence the surface waves are independent of the ground plane conductivity for this approximation.

V. Quasi-Static Approximations

In this section expressions are obtained for the fields for the quasi-static case when $k_0 \to 0$. Quasi-static approximations are obtained by noting that the term u can be written as

$$u^2 = u_0^2 - (\epsilon_r - 1)k_0^2. \tag{43}$$

Thus, the obvious simplification is to make $u = u_0$ in the Sommerfeld integrals. With this substitution, analytical evaluation is possible by series expansion and term by term integration. Introducing the variable and the parameters

$$t = \exp(-2u_0 h) \tag{44}$$

$$\epsilon_m = \frac{\epsilon_r + 1}{2} \tag{45}$$

$$\eta = \frac{\epsilon_r - 1}{\epsilon_r + 1} \tag{46}$$

it is seen that

$$\frac{1}{D_H} = \frac{1-t}{2u_0} \tag{47}$$

$$\frac{N}{D_E} = \frac{2}{(\epsilon_r + 1)(1+\eta t)} = \frac{1}{\epsilon_m}(1 - \eta t + \eta^2 t^2 + \cdots) \tag{48}$$

and hence we obtain for the integrals appearing in the electric field the expressions

$$* \int_C H_0^{(2)}(k_\rho \rho)\frac{k_\rho}{D_H} dk_\rho = \frac{\exp(-jk_0 r_0)}{r_0} - \frac{\exp(-jk_0 r_1)}{r_1} \tag{49}$$

$$* \int_C H_1^{(2)}(k_\rho \rho)\frac{k_\rho^2 N}{D_H D_E} dk_\rho = \frac{\rho}{\epsilon_M}\left[\frac{1+jk_0 r_0}{r_0^3}\exp(-jk_0 r_0) - (1+\eta) \cdot \sum_{i=1}^{\infty}(-\eta)^{i-1}\frac{1+jkr_i}{r_i^3}\exp(-jk_0 r_i)\right] \tag{50}$$

where

$$r_i = \sqrt{\rho^2 + (z+2ih)^2}, \qquad i = 0, 1, 2, \cdots \tag{51}$$

$$* \int_C H_0^{(2)}(k_\rho \rho) \frac{k_\rho^3 N}{D_H D_E} \exp(-u_0 z)\, dk_\rho = \frac{1}{\epsilon_r + 1}\left[\left(-\frac{\rho^2 Q_0}{r_0^5} + \frac{2P_0}{r_0^3}\right)\exp(-jk_0 r_0) - (1+\eta)\sum_{i=1}^{\infty}(-\eta)^{i-1} \cdot \left(-\frac{\rho^2 Q_i}{r_i^5} + \frac{2P_i}{r_i^3}\right)\exp(-jk_0 r_i)\right] \tag{52}$$

and

$$* \int_C H_1^{(2)}(k_\rho \rho) \frac{u_0 k_\rho^2 \tanh u_0 h}{D_E}\, dk_\rho = \frac{\rho}{\epsilon_r + 1}\left[\frac{zQ_0}{r_0^5}\exp(-jk_0 r_0) - (1+\eta) \cdot \sum_{i=1}^{\infty}(-\eta)^{i-1}\frac{(z+2ih)Qi}{r_i 5}\exp(-jk_0 r_i)\right] \tag{53}$$

with

$$P_i = 1 + jk_0 r_i \tag{54}$$

$$Q_i = 3 + 3jk_0 r_i - k_0^2 r_i^2. \tag{55}$$

Similar expansions can be obtained for the integrals related to the magnetic field (32)–(34). Of course when $k_0 = 0$ (zero frequency) either the exact expressions or the quasi-static approximations become the static case in which the fields are created by an electrostatic dipole of moment $qdx = Idx/j\omega$. This moment becomes infinite at zero frequency. Hence, in order to avoid computing infinite fields in the static limiting case, we shall consider that the current in the HED is proportional to the frequency, or in other words the electrostatic moment qdx remains finite at zero frequency. This assumption corresponds closely to the practical case of a dipole showing a capacitive input impedance and excited by a voltage generator.

VI. Computational Details

For the evalution of the fields, it is necessary to evaluate certain infinite integrals of oscillatory functions and divergent integrals as $\lambda \to \infty$. In addition, there exists poles near the path of integration which makes numerical integration along the real axis more complicated. For the sake of simplicity, we shall consider that the working frequency satisfies the condition $f < c_0/4h\sqrt{\epsilon_r} - 1$. Thus, only one pole, corresponding to the first zero of D_E, must be considered [11].

Numerical techniques developed for the lossless case [7] do not work accurately for all parameters of interest, particularly when there is a lossy dielectric substrate. Many new techniques have been devised and checked extensively. This section gives an outline of the numerical techniques which in our opinion are best adapted to this problem.

Even though many paths have been tried to evaluate these integrals, we felt the integration along the real axis is the most efficient. Fig. 3(a) shows a typical example of the class of function to be integrated. An enlarged view in the interval $[0.9k_0, 1.4k_0]$ is depicted in Fig. 3(b). The main difficulties regarding the numerical integration, are then infinite derivatives at $\lambda = k_0$ and the strong variations near the complex pole, especially the sharp peak in the imaginary part. Moreover, the function oscillates and diverges at infinity.

The integration interval is decomposed into three subintervals $[0, k_0]$, $[k_0, k_0\sqrt{\epsilon_r}]$ and $[k_0\sqrt{\epsilon_r}, \infty]$. In the region $[0, k_0]$ the infinite derivative in k_0 is eliminated with a change of variables $\lambda = k_0 \cos t$. The resulting smoother function is integrated numerically. In the interval $[k_0, \sqrt{\epsilon_r} k_0]$, the singularity is first extracted (if the integrand includes the denominator D_E). By writing the function under the integral sign in the form $F(\lambda) = J_n(\lambda_\rho) f(P)$, then we have

$$F(\lambda) = \left[J_n(\lambda\rho) f(\lambda) - F_{\text{sing}}(\lambda)\right] + F_{\text{sing}}(\lambda) \tag{56}$$

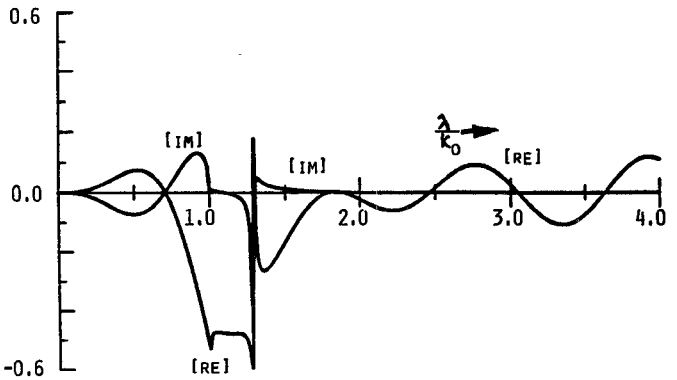

(a)

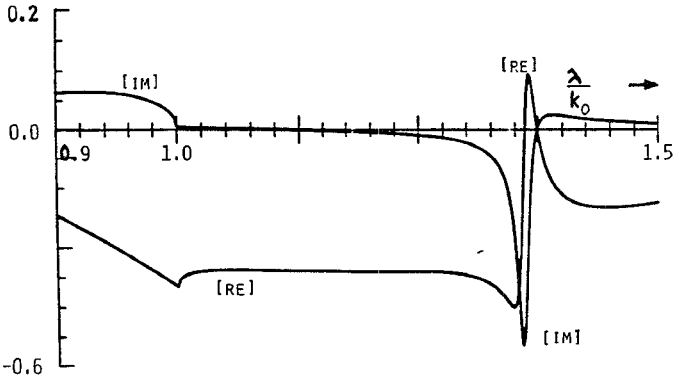

(b)

Fig. 3. (a) The complex integrand for the scalar potential. $\epsilon_r' = 5$, $\tan\theta = 0.01$, $k_{0\rho} = 5.4$, $k_0 h = 0.2\pi$. [RE] → real part of the integrand. [IM] → imaginary part of the integrand. (b) Enlarged view of the integrand for Fig. 3(a) in $[0.9k_\rho, 1.4k_\rho]$. [RE] → real part of the integrand. [IM] → imaginary part of the integrand.

where

$$F_{\text{sing}}(\lambda) = \frac{R'}{\lambda - (\lambda_p + j\nu_p)} \quad (57)$$

Here $\lambda_p + j\nu_p$ is the complex pole and R' the residue of F at the pole

$$R' = J_n\left[(\lambda_p + j\nu_p)\rho\right] \cdot \lim_{k_\rho \to \lambda_p + j\nu_p} (k_\rho - \lambda_p - j\nu_p) f(k_\rho). \quad (58)$$

The function F_{sing} is integrated analytically as

$$I_{\text{sing}} = \int_{k_0}^{k_0\sqrt{\epsilon_r}} F_{\text{sing}}\, d\lambda = \frac{R'}{2} \ln \frac{\nu_p^2 + \left(k_0\sqrt{\epsilon_r} - \lambda_p\right)^2}{\nu_p^2 + \left(k_0 + \lambda_p\right)^2} + jR' \arctan \frac{k_0\sqrt{\epsilon_r} - \lambda_p}{\nu_p} + jR' \arctan \frac{\lambda_p - k_0}{\nu_p} \quad (59)$$

and ν_p approaches zero from the negative side. It is worth mentioning that when $\nu_p \to 0$ with $\lambda_p > k_0$

$$I_{\text{sing}} = R' \ln \frac{k_0\sqrt{\epsilon_r} - \lambda_p}{\lambda_p - k_0} - j\pi R' = R' \int_{k_0}^{k_0\sqrt{\epsilon_r}} \frac{d\lambda}{\lambda - \lambda_\rho} - j\pi R' \quad (60)$$

and hence the lossless case is a special case of this general procedure.

Fig. 4 depicts the real part of the original function $F(\lambda)$ (curve A) and of the difference $F(\lambda) - F_{\text{sing}}(\lambda)$ (curve B, where the singularity has been extracted). There is still an infinite derivative in the curve B at $\lambda = k_0$. With a change of variable $\lambda = k_0 \cosh t$ one finally obtains a very smooth integrand (discontinuous line in Fig. 4), which is integrated by a Gaussian quadrature. The same procedure is applied to the imaginary part of $F(\lambda)$ to eliminate in a similar way the sharp peak and the infinite derivative.

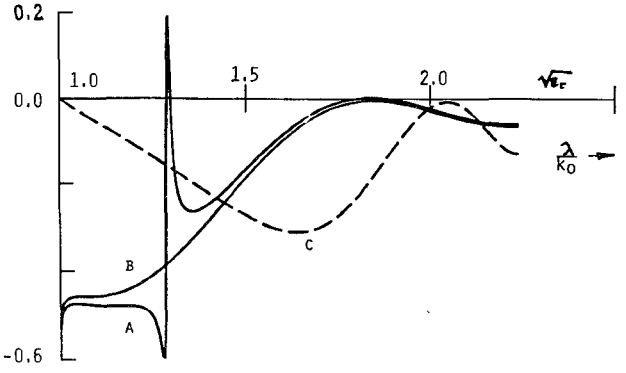

Fig. 4. The integrand of Fig. 3 (real part only) in the interval $[k_\rho, k_\rho\sqrt{\epsilon_r}]$.

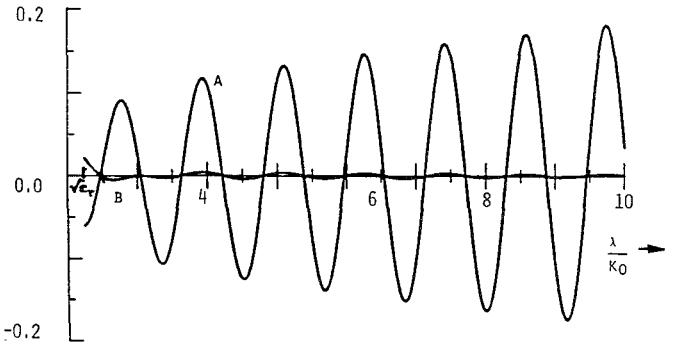

Fig. 5. The integrand of Fig. 3 (real part only) in the interval $[k_\rho\sqrt{\epsilon_r}, 10k_\rho]$.

Finally, in the region $[\sqrt{\epsilon_r}k_0, \infty]$ we first extract the static term defined by $F(\lambda, k_0 = 0)$. Fig. 5 depicts the integrand $F(\lambda, k_0)$ (curve A) and the difference $F(\lambda, k_0) - F(\lambda, 0)$ (curve B). It can be shown that the static term has the form

$$F(\lambda, k_0 = 0) = CJ_n(\lambda\rho)\lambda^m \quad (61)$$

and hence it can be integrated analytically.

The remaining part is a slowly convergent oscillating function which is handled with a specially tailored numerical technique [7]. Extensive tests have been performed to check the validity of the numerical results in the range $0.001 \le k_0\rho \le 100$, $0.01 \le k_0 h \le 1.5$, $1 \le \epsilon_r \le 10$ and for different ground plane conductivities and dielectric losses. Typical results are presented in the next section.

VII. Results

To allow a quantitative comparison between static and dynamical fields, we have introduced a "dynamical factor Q_i" defined as the ratio between the modulus of the dynamical field value (complex) and the corresponding static field value (real) at the same point

$$Q_i = |E_i(\text{DYN})|/E_i(\text{STAT}) \quad (62)$$

where i stands for any cartesian component x, y, z. Obviously, Q_i must approach the unity as frequency approaches zero.

Static values in (62) have been computed form expressions (49)–(55), in the limiting case $k_0 = 0$. In the limit $k_0 = 0$, an infinite series arises in these expressions. The sum of that series has been obtained by applying the well-known Shanks nonlinear transformation [12]. Dynamic values have been found by evaluating the integrals (29)–(34) with the techniques of Section VI.

The results presented here concern the x-component of the electric field in the interface, calculated along the dipole axis, i.e., for $\phi = 0°$. Data for other directions or components can be obtained in a similar way.

Fig. 6 shows the dynamical factor Q_x for a microstrip lossless substrate with $\epsilon_r = 2$ and thickness $h = 3$ mm. Three frequencies, namely 1, 5, and 10 GHz, have been investigated for source-observer distances ranging between

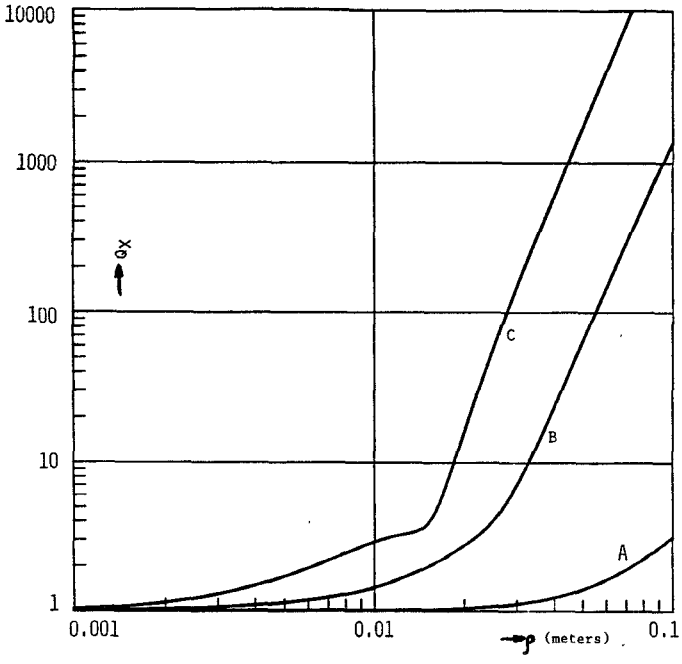

Fig. 6. Effect of frequency on the dynamical factor Q_x as a function of ρ for the parameters $\epsilon_r = 2$, $\tan\theta = 0$, $h = 3$ mm. 6*A*: $f = 1$ GHz. 6*B*: $f = 5$ GHz. 6*C*: $f = 10$ GHz.

1 and 100 mm. The values of Q_x depend strongly on frequency. However, similar values are obtained at different frequencies if distances are measured in free-space wavelengths.

Fig. 7 corresponds to the cases represented in Fig. 6 but the dynamical factor is now plotted against normalized distances. For instance, at $0.1\lambda_0$ from the source, the ratio Q_x is 1.1 at 1 GHz and 1.3 at 10 GHz.

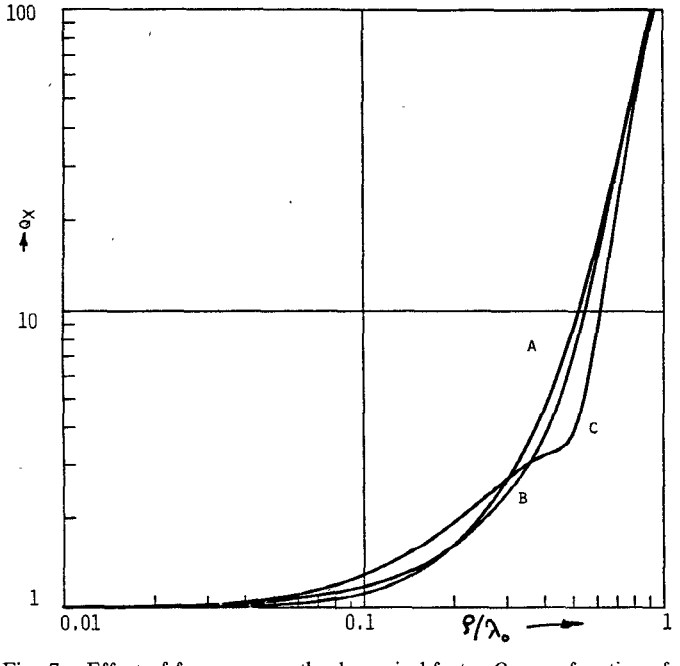

Fig. 7. Effect of frequency on the dynamical factor Q_x as a function of the normalized distance for the parameters $\epsilon_r = 2$, $\tan\theta = 0$, $h = 3$ mm. 7*A*: $f = 1$ GHz. 7*B*: $f = 5$ GHz. 7*C*: $f = 10$ GHz.

In Fig. 8, a higher dielectric constant has been considered with the remaining parameters unchanged. At 1 GHz, the dynamical factor remains close to unity and even slightly smaller until a distance $0.1\lambda_0$.

Then it increases very quickly. For higher frequencies, static approximations are barely useful, the dynamical factor being 1.35 at 5 GHz and 1.75 at 10 GHz.

The effect of permittivity is examined in Fig. 9. The normalized substrate thickness is very small ($h/\lambda_0 =$

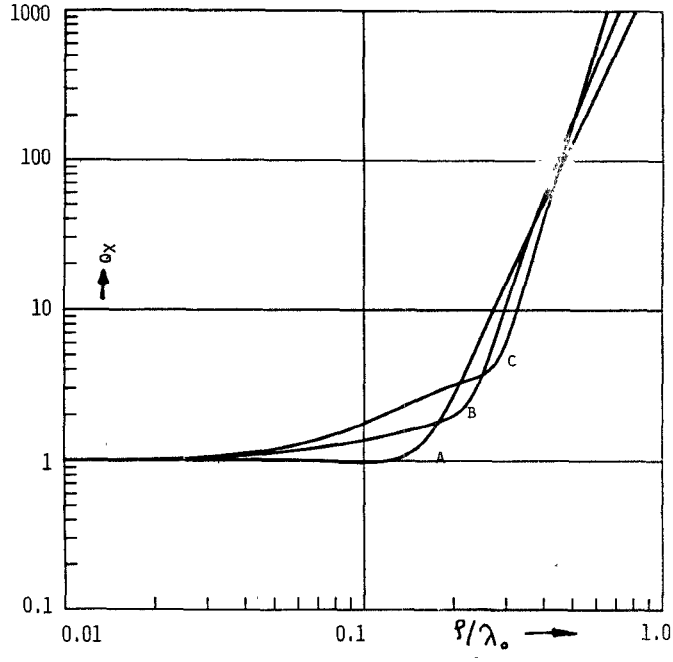

Fig. 8. Effect of frequency on the dynamical factor Q_x for a higher permittivity $\epsilon_r = 5$, $\tan\theta = 0$, $h = 3$ mm. 8*A*: $f = 1$ GHz. 8*B*: $f = 5$ GHz. 8*C*: $f = 10$ GHz.

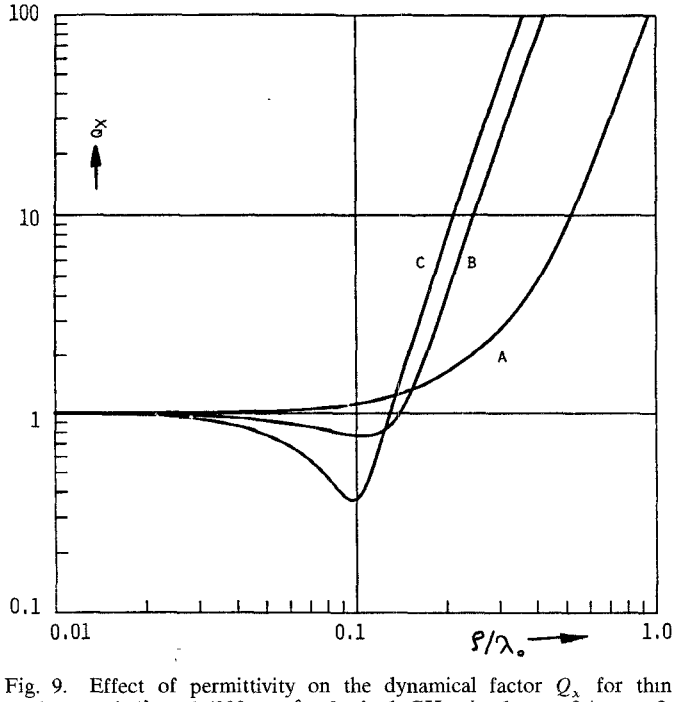

Fig. 9. Effect of permittivity on the dynamical factor Q_x for thin substrate $h/\lambda_0 = 1/300$. $\tan\theta = 0$, $f = 1$ GHz, $h = 1$ mm. 9*A*: $\epsilon_r = 2$. 9*B*: $\epsilon_r = 6$. 9*C*: $\epsilon_r = 8$.

1/300). The dynamical factor has a very interesting behaviour for high permittivity. It remains below unity for a wide range of distances. For instance, for $\epsilon_r = 8$, the dynamical field is only 35 percent of the static value at $\rho/\lambda_0 = 0.1$. These phenomena disappear in thicker substrates as evidenced by Fig. 10 where $h/\lambda_0 = 1/20$. In this case, Q_x remains always greater than unity.

The dependence of the dynamical factor with substrate thickness has been depicted in Figs. 11 and 12. For thin substrates (Fig. 11), Q_x exhibits similar behavior as discussed in preceding figures. It remains nearly constant or increases very slowly until a critical distance (between $0.1\lambda_0$ and $0.2\lambda_0$ in the examples considered) is reached. For greater distances, the dynamical factor increases very quickly and values between 10^3 and 10^4 are obtained at $\rho = \lambda_0$.

The distances considered in the above eases correspond to a near field zone, where the true field is dominated by

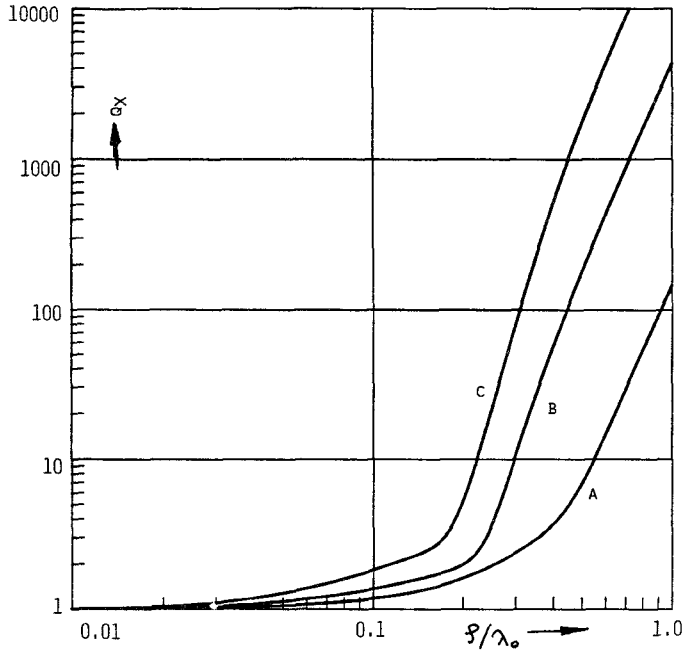

Fig. 10. Effect of permittivity on the dynamical factor Q_x for a thick substrate $h/\lambda_0 = 1/20$. $\tan\theta = 0$, $f = 5$ GHz, $h = 3$ mm. 10*A*: $\epsilon_r = 2$. 10*B*: $\epsilon_r = 5$. 10*C*: $\epsilon_r = 10$.

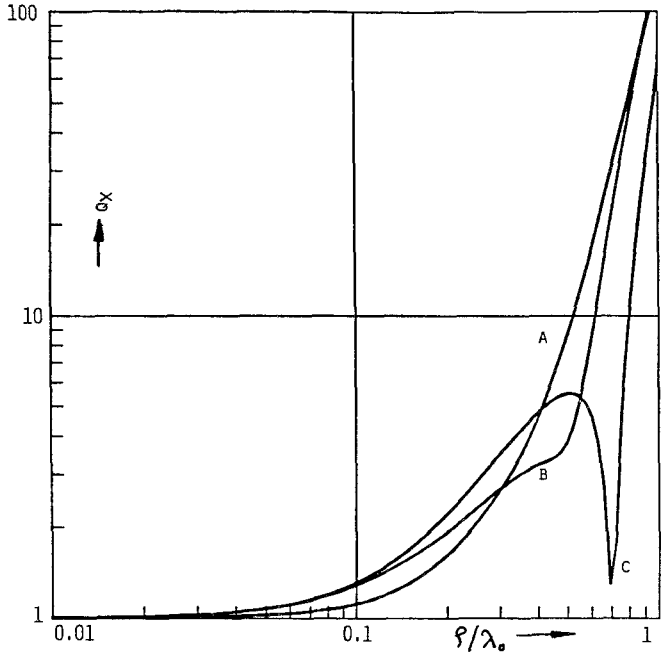

Fig. 12. Effect of substrate thickness on the dynamical factor Q_x for high normalized thickness. $\epsilon_r = 2$, $f = 1$ GHz, $\tan\theta = 0$. 12*A*: $h = 3$ mm 12*B*: $h = 30$ mm 12*C*: $h = 60$ mm.

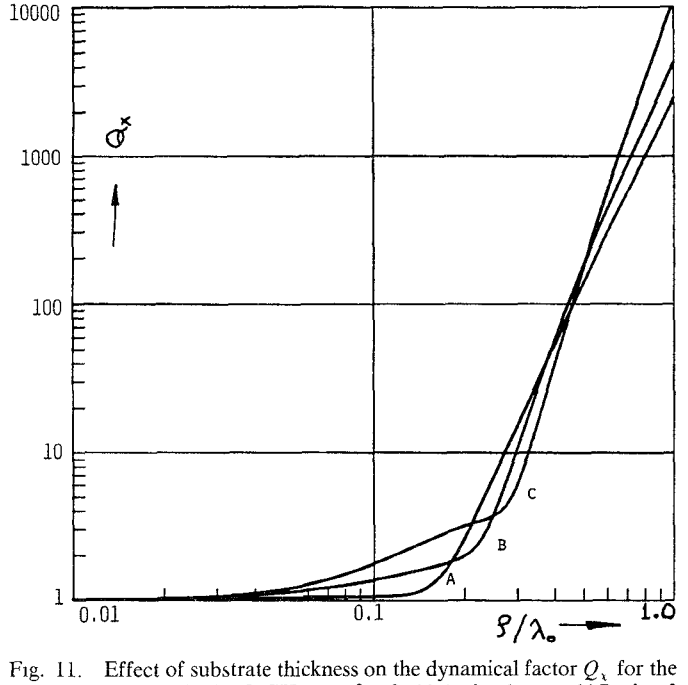

Fig. 11. Effect of substrate thickness on the dynamical factor Q_x for the parameters $\epsilon_r = 5$, $f = 5$ GHz, $\tan\theta = 0$ 11*A*: $h = 1$ mm. 11*B*: $h = 3$ mm. 11*C*: $h = 6$ mm.

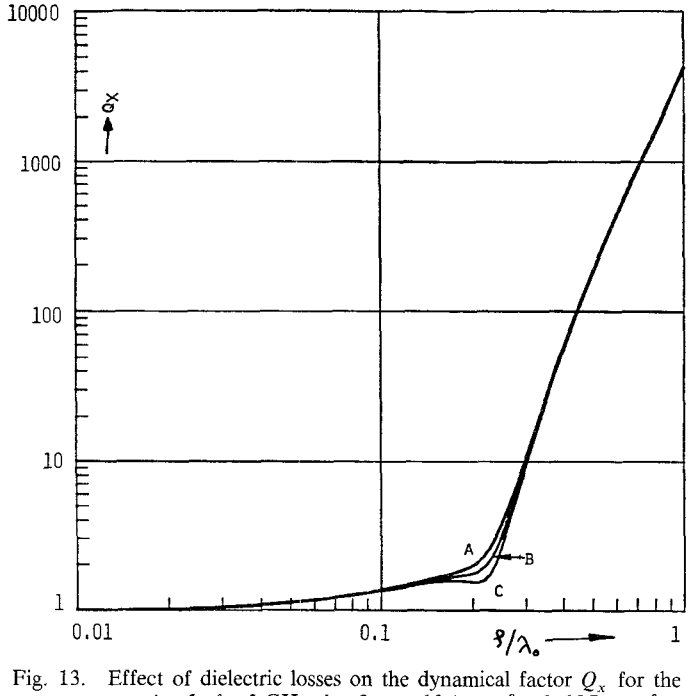

Fig. 13. Effect of dielectric losses on the dynamical factor Q_x for the parameters. $\epsilon_r' = 5$, $f = 5$ GHz, $h = 3$ mm. 13*A*: $\tan\theta = 0$. 13*B*: $\tan\theta = 0.1$. 13*C*. $\tan\theta = 0.2$.

the quasi-static term. The quasi-static term decreases as ρ^{-3}, and in the dynamical zone the surface wave takes over. There the field decays as $\rho^{-1/2}$. For thicker substrates (Fig. 12) an interesting phenomenon appears. The dynamical factor is always greater than unity, but it can exhibit a sudden decrease in the form of a narrow deep valley. In Fig. 12 with $h/\lambda_0 = 0.2$ and $\epsilon_r = 2$ (curve C) we obtain $Q_x = 1.3$ for $\rho = 0.7\lambda_0$ while values above $Q_x = 5$ are obtained at $0.6\lambda_0$ and $0.8\lambda_0$.

Figure 13 shows the relevance of dielectric losses. In the range $0 < \tan\theta < 0.2$, the effect of a lossy substrate is seldom noticeable except for points in the neighborhood of the transition zone.

The effect of a finite ground plane conductivity has also been studied. No significant differences have been found as far as conductivities remains above 10^6 S/m or surface impedances below 0.5 Ω.

VIII. Conclusions

In this paper we have compared the quasi-static solution with the exact solution for the fields of an horizontal electric dipole located over a lossy dielectric and backed by an imperfectly conducting ground plane.

Theoretical expressions for the six components of the electromagnetic field have been derived, and the numerical techniques needed for their evaluation have been outlined. As an application, we give practical results for the tangential component of the electric field parallel to the dipole.

It is found that the region of validity of the quasi-static solution depends critically on substrate thickness and dielectric constant, whereas ohmic and dielectric losses have only a weak influence. In general, the quasi-static approximation underestimates the strength of the fields. However, particular combinations of substrate parameters and frequency can yield anomalous situations where the true values are well below the quasi-static predictions.

The results presented here can be generalized by superposition to the study of any microstrip structure. In particular, coupled lines may be analyzed by an integral equation approach in which the Green's functions may be constructed from the field expressions presented in this paper. Work in this direction is in progress and will be reported in coming paper.

References

[1] J. R. Wait, *Electromagnetic Waves in Stratified Media*. New York: Pergamon Press, 1970.

[2] L. B. Felsen and N. Marcuvitz, *Radiation and Scattering of Waves*. Engelwood Cliffs, NJ: Prentice Hall, 1973.

[3] J. A. Kong, *Theory of Electromagnetic Waves*. New York: John Wiley and Sons, 1975.

[4] J. A. Kong, "Antenna radiation in stratified media," in *Research Topics in Electromagnetic Theory*. New York: Pergamon Press, 1981.

[5] H. A. Haddad and D. C. Chang, "Dyadic Green's function for a two layered earth," Air Force Weapons Lab, Kirtland AFB, AFWL-TR-77-69, 1977.

[6] N. K. Uzunoglu, N. Alexopoulos, and J. G. Fikioris, "Radiation properties of microstrip dipolies," *IEEE Trans. Antennas Propagat.*, vol. AP-27, pp. 853–858, 1979.

[7] J. R. Mosig and F. E. Gardiol, "Analytic and numerical techniques in the Green's function treatment of microstrip antennas and scatterers," *Proc. IEE*, part H (MOA), vol. 130, pp. 175–182, 1983.

[8] J. R. Wait, "Fields of a horizontal dipole over a stratified anisotropic half-space," *IEEE Trans. Antennas Propagat.*, vol. AP-14, pp. 790–792, 1966.

[9] L. Tsang and J. L. Kong, "Electromagnetic fields due to a horizontal electric dipole antenna laid on the surface of a two layered medium, *IEEE Trans. Antennas Propagat.*, vol. AP–22, pp. 709–711, 1974.

[10] R. F. Harrington, *Time Harmonic Electromagnetic Fields*. New York: McGraw Hill, 1961.

[11] J. R. Mosig and F. E. Gardiol, "A dynamical radiation model for microstrip structures," in *Advances in Electronics and Electron Physics*, vol. 59, P. Hawkes, Ed. New York: Acedemic Press, pp. 139–237, 1982.

[12] D. Shanks, "Non-linear transformations of divergent and slowly convergent sequences," *J. Math. Phys.*, vol. 34, pp. 1–42, 1955.

✠

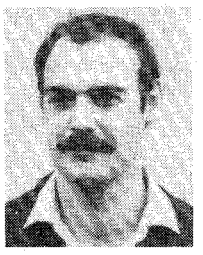

Juan R. Mosig was born in Cadiz, Spain on December 18, 1951. He received the Electrical Engineer degree in 1973 from Universidad Politecnica de Madrid. In 1975 he joined the Laboratory of Electromagnetics and Acoustics of the Ecole Polytechnique Fédérale de Lausanne, Switzerland from which he obtained the Ph.D. Degree in 1983. In 1984 he was a Visiting Research Associate at Rochester Institute of Technology, NY. He is currently a Senior Assistant at Ecole Polytechnique Fédérale. His research interests include electromagnetic theory, numerical methods and microstrip antennas.

✠

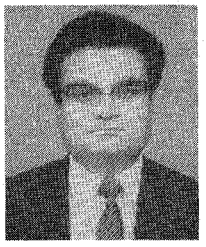

Tapan K. Sarkar (S'69–M'76–SM'81) was born in Calcutta, India, on August 2, 1948. He received the B. Tech. degree from the Indian Institute of Technology, Kharagpur, India, in 1969, the M.Sc.E. degree from the University of New Brunswick, Fredericton, NB, Canada, in 1971, and the M.S. and Ph.D. degrees from the Syracuse University, Syracuse, NY, in 1975.

From 1969 to 1971, he served as an Instructor at the University of New Brunswick. While studying at Syracuse University, he served as an Instructor and Research Assistant in the Department of Electrical Engineering. From 1976 to 1985, he was with Rochester Institute of Technology, Rochester, NY. From 1977 to 1978, he was a Research Fellow at the Gordon McKay Laboratory of Harvard University, Cambridge, MA. Presently, he is with the Department of Electrical and Computer Engineering of Syracuse University, Syracuse, NY. His current research interest deal with numerical solution of operator equations arising in electromagnetics and signal processing with application to system identification.

Dr. Sarkar is a Registered Professional Engineer in the state of New York. He is a member of Sigma Xi and International Union of Radio Science Commissions A and B.